

Navigating surface reconstruction of spinel oxides for electrochemical water oxidation

Received: 20 September 2022

Accepted: 11 April 2023

Published online: 28 April 2023

Check for updates

Yuanmiao Sun^{1,2,12}, Jiarui Wang^{3,4,12}, Shibo Xi^{5,12}, Jingjing Shen³,
Songzhu Luo³, Jingjie Ge⁶, Shengnan Sun⁷, Yubo Chen³,
John V. Hanna^{3,8}, Shuzhou Li³, Xin Wang⁹ & Zhichuan J. Xu^{3,10,11} ✉

Understanding and mastering the structural evolution of water oxidation electrocatalysts lays the foundation to finetune their catalytic activity. Herein, we demonstrate that surface reconstruction of spinel oxides originates from the metal-oxygen covalency polarity in the M_T-O-M_O backbone. A stronger M_O-O covalency relative to M_T-O covalency is found beneficial for a more thorough reconstruction towards oxyhydroxides. The structure-reconstruction relationship allows precise prediction of the reconstruction ability of spinel pre-catalysts, based on which the reconstruction degree towards the in situ generated oxyhydroxides can be controlled. The investigations of oxyhydroxides generated from spinel pre-catalysts with the same reconstruction ability provide guidelines to navigate the cation selection in spinel pre-catalysts design. This work reveals the fundamentals for manipulating the surface reconstruction of spinel pre-catalysts for water oxidation.

The increasing global energy consumption and depletion of fossil fuels have necessitated the establishment of a sustainable and environmentally friendly energy cycle. Hydrogen has been expected to be an ideal solution because of its renewability, high energy density, and clean exhaust products¹. Among various hydrogen production techniques, electrochemical water splitting offers a green method to directly generate hydrogen using electricity, which can be acquired from renewable sources such as wind, tides, and sunlight. However, the overall efficiency of water splitting is largely hindered by the sluggish oxygen evolution reaction (OER) at the anode, which makes the design of efficient OER catalysts an urgent issue^{2,3}.

Rational catalyst design calls for a comprehensive understanding of the reaction process, based on which key reaction fundamentals can be summarized to aid the design of remarkable catalyst. For example, it has been long recognized that the adsorption of reaction intermediates on the active sites plays important role in determining the activity³⁻⁵. Based on this, oxide $IrO_x/SrIrO_3$ and perovskite $Ba_{0.5}Sr_{0.5}Co_{0.8}Fe_{0.2}O_{3-d}$ (BSCF) have been designed, which exhibit neither too strong nor too weak binding affinity to the oxygen-related intermediates^{6,7}. More recently, the surface reconstruction of electrocatalysts under electro-oxidation conditions has been widely detected⁸⁻¹⁰. Surface reconstruction leads to in situ formation of a

¹Faculty of Materials Science and Energy Engineering/Institute of Technology for Carbon Neutrality, Shenzhen Institute of Advanced Technology, Chinese Academy of Sciences, Shenzhen 518055, P. R. China. ²Shenzhen Key Laboratory of Energy Materials for Carbon Neutrality, Shenzhen Institute of Advanced Technology, Chinese Academy of Sciences, Shenzhen 518055, P. R. China. ³School of Materials Science and Engineering, Nanyang Technological University, 50 Nanyang Avenue, Singapore 639798, Singapore. ⁴Singapore-HUJ Alliance for Research and Enterprise (SHARE), NEW-CREATE Phase II, Campus for Research Excellence and Technological Enterprise (CREATE), Singapore 138602, Singapore. ⁵Institute of Chemical and Engineering Science, Agency for Science Technology and Research (A*Star), Singapore 627833, Singapore. ⁶Department of Chemical and Biological Engineering, HKUST Jockey Club Institute for Advanced Study, Energy Institute, The Hong Kong University of Science and Technology, Clear Water Bay/Kowloon Hong Kong, China. ⁷Institute of Materials Research and Engineering (IMRE), Agency for Science, Technology and Research (A*Star), 2 Fusionopolis Way, Innovis #08-03, Singapore 138634, Republic of Singapore. ⁸Department of Physics, University of Warwick, Coventry, UK. ⁹Department of Chemistry, City University of Hong Kong, Hong Kong, China. ¹⁰Energy Research Institute @ Nanyang Technological University, ERI@N, Interdisciplinary Graduate School, Nanyang Technological University, 50 Nanyang Avenue, Singapore 639798, Singapore. ¹¹Center for Advanced Catalysis Science and Technology, Nanyang Technological University, 50 Nanyang Avenue, Singapore 639798, Singapore. ¹²These authors contributed equally: Yuanmiao Sun, Jiarui Wang and Shibo Xi. ✉ e-mail: xuzc@ntu.edu.sg

core-shell structure, in which the oxyhydroxides in the surface and near-surface region are considered as the real catalytic species for the reaction. This paves the way for new design paradigm to manipulate the surface reconstruction of pre-catalyst for advanced OER activity. However, to date studies about surface reconstruction mainly focus on exploring the compositional effect on the activity of the reconstructed oxyhydroxides;^{11,12} it remains unclear in which way and to what extent we can control the surface reconstruction of pre-catalyst.

A prerequisite to manipulate surface reconstruction is to identify what triggers the process of surface reconstruction. Some pioneer works recommend cation leaching as the origin of surface reconstruction^{8,13,14}. For example, lithium cation is considered unstable in alkaline conditions and therefore can easily leach out to activate surface reconstruction. J. Wang et al. have achieved severe in situ reconstruction in layered $\text{LiCoO}_{2-x}\text{Cl}_x$ ($x = 0, 0.1$ and 0.2) due to lithium leaching¹⁴. However, no such reconstruction was observed in spinel LiMn_2O_4 , where lithium cations are intensively involved but the spinel framework remains almost unchanged during OER^{15,16}. The contradictory phenomena suggest that the leaching of metal cations is not element-dependent but should be material-dependent, which necessitates deeper investigations into the electronic structures to give an explicit explanation. Unfortunately, this part has been less touched and remains elusive. Besides, precise control of the reconstruction ability of pre-catalyst is demanded. Surface reconstruction may not always bring activity enhancement. If the intrinsic activity of pre-catalyst is superior to that of the reconstructed counterpart, strategies should be made to suppress the reconstruction to guarantee a long reaction durability. On the contrary, if the reconstructed oxyhydroxide shows superior activity, the pre-catalyst should be designed with high reconstruction ability to promote surface reconstruction. This calls for the establishment of a structure-reconstruction relationship, based on which the reconstruction ability of pre-catalyst can be forecasted and finetuned. In addition, principles are needed to guide the selection of metal cations in the design of pre-catalyst. The activity of the reconstructed oxyhydroxides is dependent on the type and ratio of metal cations¹¹. Therefore, to facilitate in situ generation of highly active oxyhydroxides, investigations are intensively needed to pinpoint the active cation species in reconstructed oxyhydroxides.

Herein, using spinel $\text{Li}_x\text{Co}_{1-x}\text{Co}_2\text{O}_4$ as model catalysts, we demonstrate that surface reconstruction of spinel oxides originates from the biased metal-oxygen covalency between MO_4 and MO_6 . Combining computational and experimental approaches, a structure-reconstruction relationship has been established, based on which the reconstruction ability of spinel pre-catalyst can be effectively forecasted. Further electrochemical analysis and computational calculations deliver some useful clues for the cation selection in spinel pre-catalysts. This work unveils the structural origin of reconstruction for spinel oxides. It also provides a structure-reconstruction relationship applicable to all spinel family to forecast their reconstruction ability. The demonstrated strategies to master surface reconstruction provides firm theoretical foundations to navigate the design of spinel pre-catalysts with controllable reconstruction ability for electrochemical water oxidation.

Results and discussions

Theoretical investigation of the structural origin of surface reconstruction on spinel oxides

The structural composition of spinel oxides is AB_2O_4 , in which the cations in A sites and B sites are tetrahedrally and octahedrally coordinated, respectively. Within the structure, the octahedral units connect to one another via an edge-shared form, while the connection between tetrahedral units and octahedral units is corner-shared (Fig. 1a). The oxygen ligands are arranged in a cubic close-packed lattice and each of them is shared by three octahedral cations and one tetrahedral cation to create a $\text{M}_T\text{-O-M}_O$ backbone¹⁷. When catalyzing

OER, the spinel frame may collapse and reconstruct to amorphous oxyhydroxides during electrochemical cycling. The evolution from spinel to amorphous oxyhydroxides necessitates the breakage between the tetrahedral and octahedral units, during which highly reactive and transferrable oxygen ligands are believed to facilitate the phase transformation. Besides, because the cations in the reconstructed oxyhydroxides stay in an octahedral coordination environment, a stronger metal-oxygen covalency of the octahedral units than the tetrahedral units may be advantageous for the reconstruction process. In other words, a biased $\text{M}_T\text{-O-M}_O$ backbone with oxygen binds more strongly to the octahedral cations may be decisive for more smoothly and thoroughly reconstructed oxyhydroxides.

To verify above hypotheses, a case study is performed on spinel $(\text{Co}_{1-x}\text{Li}_x)\text{Co}_2\text{O}_4$ ($x = 0, 0.25, 0.5, 0.75$ and 1). Spinel $(\text{Co}_{1-x}\text{Li}_x)\text{Co}_2\text{O}_4$ is chosen because the CoO_6 units are the only catalytically active centers after reconstruction, which allows us to explicitly analyze the degree of surface reconstruction. The density functional theory (DFT) calculations are carried out to explore the electronic structure evolution with the change of spinel composition. As a prerequisite for structural collapse, the reactivity of oxygen ligands is first examined. With the increase of lithium in spinel $(\text{Co}_{1-x}\text{Li}_x)\text{Co}_2\text{O}_4$, the oxygen p -band center gradually increases and moves closer to the Fermi level (Fig. 1b), indicating the oxygen ligands are becoming more active. Meanwhile, the calculated oxygen vacancy formation energy ($E_{\text{vac-O}}$) of CoCo_2O_4 is as high as 5.20 eV, suggesting severe difficulty of generating an oxygen vacancy in the structure. With the tetrahedral cobalt cations being replaced by lithium cations, the energy required to generate oxygen vacancy steadily decreases (Fig. 1c). The value of $E_{\text{vac-O}}$ decreases to 0.80 eV in LiCo_2O_4 , implying high mobility of oxygen ligands to escape from the spinel lattice. The trends of oxygen p -band center and oxygen vacancy formation energy demonstrate an activation effect to the oxygen ligands with the increase of lithium in spinel $(\text{Co}_{1-x}\text{Li}_x)\text{Co}_2\text{O}_4$.

The M–O bond strength of the $\text{M}_T\text{-O-M}_O$ backbone is subsequently evaluated by calculating the metal-oxygen covalency in the spinel structure. The metal-oxygen covalency is defined as the difference in band center between oxygen p -orbitals and metal d -orbitals, in which a higher value represents a weaker covalency¹⁷. As shown in Fig. 1d, the metal-oxygen covalency of tetrahedral units and octahedral units are quite close to each other in spinel CoCo_2O_4 and $(\text{Co}_{0.75}\text{Li}_{0.25})\text{Co}_2\text{O}_4$. In this case, oxygen binds equally to the tetrahedral and octahedral cations, which fabricates a nonpolar $\text{M}_T\text{-O-M}_O$ backbone. The spinel frame is therefore stable and should be difficult to collapse for reconstruction. However, with more lithium cations being introduced into the spinel lattice, the metal-oxygen covalency of tetrahedral and octahedral units begins to get weakened and strengthened, respectively. In spinel $(\text{Co}_{0.5}\text{Li}_{0.5})\text{Co}_2\text{O}_4$, the covalency of MO_4 units is weaker than that of MO_6 units, suggesting a biased $\text{M}_T\text{-O-M}_O$ has evolved. Compared to CoCo_2O_4 and $(\text{Co}_{0.75}\text{Li}_{0.25})\text{Co}_2\text{O}_4$, this spinel structure becomes meta-stable and the process of oxyhydroxides generation may be facilitated. The metal-oxygen covalency gap between MO_4 and MO_6 is further widened in spinel $(\text{Co}_{0.25}\text{Li}_{0.75})\text{Co}_2\text{O}_4$ and LiCo_2O_4 . In spinel LiCo_2O_4 , the calculated covalency gap is as high as 11.03 eV, implying the spinel frame is highly unstable and the reconstruction to octahedrally coordinated oxyhydroxides is considerably feasible. To further investigate the trend of surface reconstruction ability in spinel $(\text{Co}_{1-x}\text{Li}_x)\text{Co}_2\text{O}_4$, the surface transformation energy from spinel to layered oxide is calculated. The surface transformation energy is defined as the energy of (111) spinel surface relative to that of the layered CoOO species (more details are summarized in Methods). As shown in Fig. 1e, the surface transformation energy of spinel CoCo_2O_4 and $(\text{Co}_{0.75}\text{Li}_{0.25})\text{Co}_2\text{O}_4$ is far above 0 eV, suggesting the transformation from spinel to layered species is difficult. With more lithium cations substituting cobalt cations, the energy (per surface area) needed to transform spinel to layered structure gradually decreases. This indicates the difficulty for surface reconstruction is reduced. In spinel

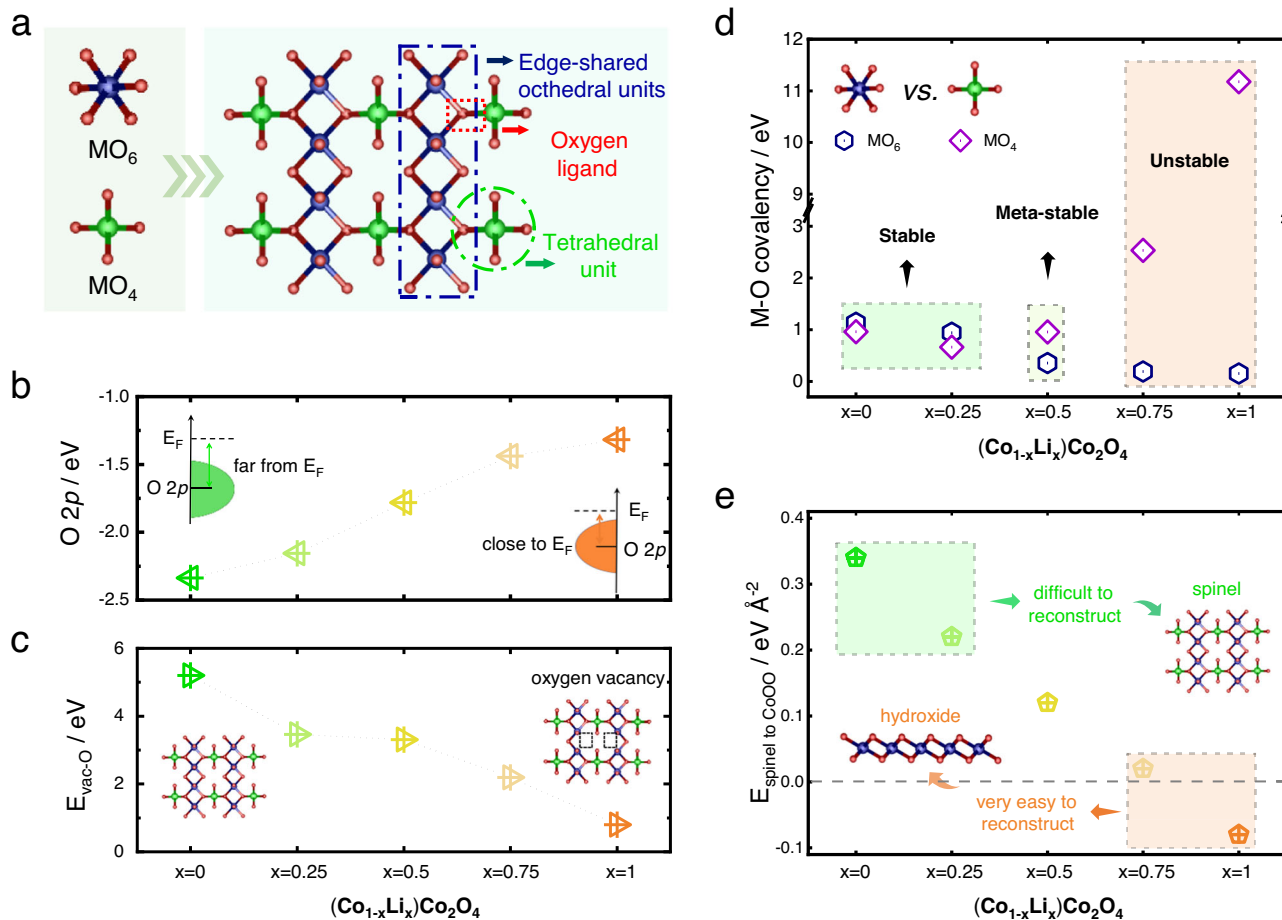


Fig. 1 | DFT investigations of the electronic structure evolution of spinel $(\text{Co}_{1-x}\text{Li}_x)\text{Co}_2\text{O}_4$ ($x = 0, 0.25, 0.5, 0.75$ and 1). **a** Illustration of the spinel AB_2O_4 structure that composed of tetrahedral units (MO_4) and octahedral units (MO_6). **b** Calculated oxygen p-band center of spinel $(\text{Co}_{1-x}\text{Li}_x)\text{Co}_2\text{O}_4$ ($x = 0, 0.25, 0.5, 0.75$

and 1). **c** Calculated vacancy formation energy ($E_{\text{O-vac}}$) of spinel $(\text{Co}_{1-x}\text{Li}_x)\text{Co}_2\text{O}_4$ ($x = 0, 0.25, 0.5, 0.75$ and 1). **d** Metal-oxygen covalency of the MO_4 and MO_6 units in spinel $(\text{Co}_{1-x}\text{Li}_x)\text{Co}_2\text{O}_4$ ($x = 0, 0.25, 0.5, 0.75$ and 1). **e** The surface transformation energy ($E_{\text{spinel to CoOO}}$) from spinel to layered species.

$(\text{Co}_{0.25}\text{Li}_{0.75})\text{Co}_2\text{O}_4$ and LiCo_2O_4 , the surface transformation energy is quite close to and even smaller than 0 eV, hinting very easy-going surface reconstruction. Therefore, we can rationally deduce that the increase of lithium cations in spinel $(\text{Co}_{1-x}\text{Li}_x)\text{Co}_2\text{O}_4$ will result in enhanced surface reconstruction ability.

Synthesis and structural characterizations of spinel $\text{Li}_x\text{Co}_{3-x}\text{O}_4$

To verify the reconstruction trend predicted by DFT calculations, spinel $\text{Li}_x\text{Co}_{3-x}\text{O}_4$ ($x = 0, 0.25, 0.5, 0.75$, and 1) were prepared by a nitrate decomposition method followed by heat treatment (more details are summarized in Methods). The inductively coupled plasma optical emission spectrometry (ICP-OES) results (Supplementary Table 1) confirm that all the as-prepared samples remain stoichiometric $\text{Li}_x\text{Co}_{3-x}\text{O}_4$. The Li $1s$ XPS spectra of the pristine samples and the derived lithium molar ratio are summarized in Supplementary Figure 1. The results evidence that, although slightly leached, the surface lithium concentration still obeys the same trend as the total lithium concentration. The crystal structure of the as-prepared spinel $\text{Li}_x\text{Co}_{3-x}\text{O}_4$ was confirmed by X-ray diffraction (XRD) analysis. As shown in Fig. 2a, the diffraction peaks of the as-prepared samples match well with that of the standard Co_3O_4 (PDF#00-042-1467), indicative of typical cubic spinel structure. The peak at 19° gets intensified with the increase of lithium in spinel $\text{Li}_x\text{Co}_{3-x}\text{O}_4$, suggesting the gradual decrease of tetrahedral cobalt cations and that the introduced lithium cations mainly reside in the tetrahedral sites¹⁸. The X-ray photoelectron spectroscopy (XPS) was performed to further evaluate the surface $\text{Co}^{2+}/\text{Co}^{3+}$ ratio of the

samples. The Co $2p$ spectrum exhibits two major peaks at 795 eV and 780 eV, ascribed to the typical Co $2p_{1/2}$ and Co $2p_{3/2}$ orbitals, respectively. An approximate energy variation of 15 eV is observed between the two major peaks, consistent with that reported in previous studies^{19,20}. The deconvolution of the two major peaks shows two characteristic peaks, which can be ascribed to Co^{2+} and Co^{3+} , respectively. As displayed in Fig. 2b, with more lithium cations substituting cobalt cations, the relative intensity of Co^{2+} characteristic peak gradually decreases, indicating the decrease of Co^{2+} cations and an increase of cobalt oxidation state. The quantitative atomic ratio of $\text{Co}^{2+}/\text{Co}^{3+}$ could be estimated by comparing the area of the characteristic peaks¹⁹. The results, which are given in Supplementary Table 2, show an obvious decrease of the surface $\text{Co}^{2+}/\text{Co}^{3+}$ ratio, further hinting the occupation of lithium cations in the tetrahedral sites.

The Fourier Transform Infrared (FTIR) spectroscopy was employed to probe the local chemical bond change of the as-prepared samples (Fig. 2c). The bands in the frequency range from 500 cm^{-1} to 700 cm^{-1} are attributed to the vibrations of the CoO_6 octahedra²¹. Specifically, the one at around 570 cm^{-1} is attributed to the asymmetric stretching modes of CoO_6 and the one at around 670 cm^{-1} to the bending modes of Co-O-Co²¹. The band at around 448 cm^{-1} corresponds to the stretching vibrations of LiO_4 tetrahedra²². This characteristic band gets intensified with the increase of Li in spinel $\text{Li}_x\text{Co}_{3-x}\text{O}_4$, which indicates, once again, the residence of lithium cations in the tetrahedral sites. The cation occupancy was also confirmed by the extended X-ray absorption fine structure (EXAFS)

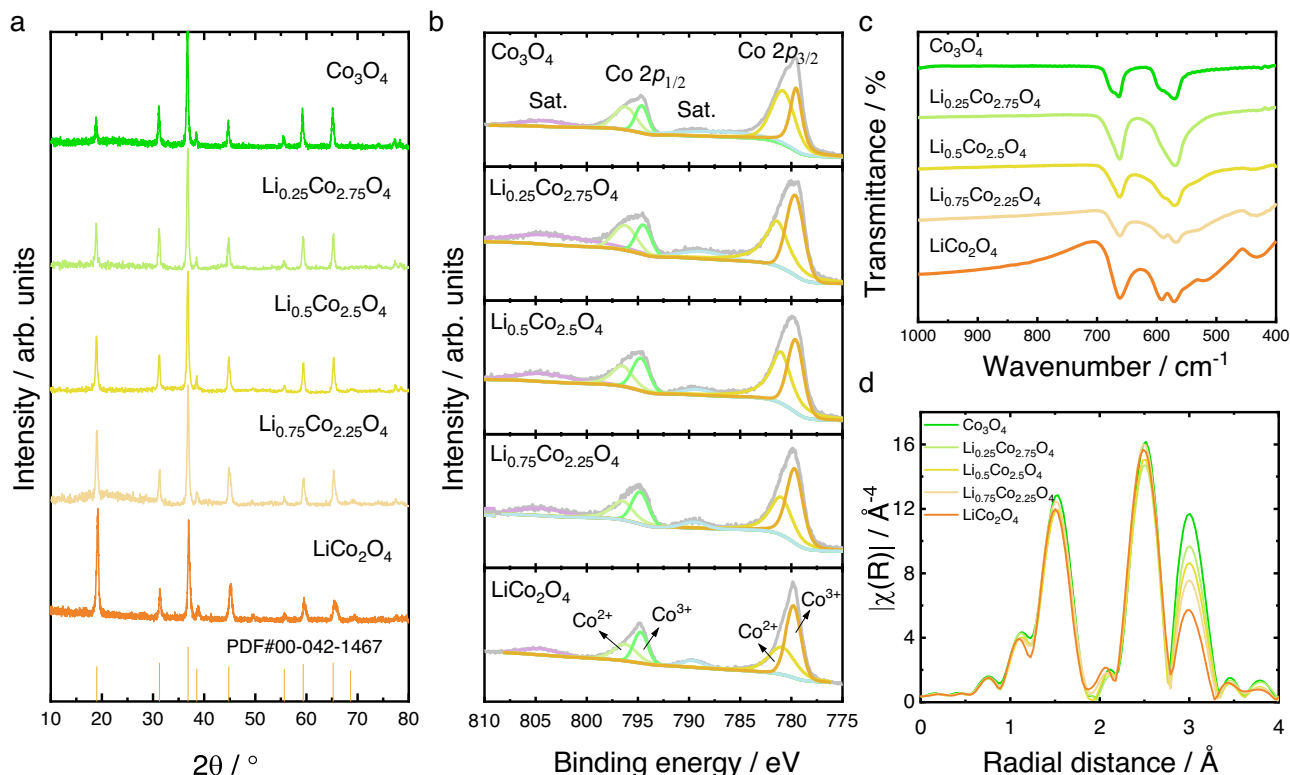


Fig. 2 | Structural characterization of the as-prepared spinel $\text{Li}_x\text{Co}_{3-x}\text{O}_4$. **a** X-ray diffraction (XRD) patterns of the as-prepared spinel $\text{Li}_x\text{Co}_{3-x}\text{O}_4$ samples. **b** The Co 2p X-ray photoelectron spectroscopy (XPS) spectra of the as-prepared spinel $\text{Li}_x\text{Co}_{3-x}\text{O}_4$ samples. **c** The Fourier Transform Infrared (FTIR) spectra of the as-

prepared spinel $\text{Li}_x\text{Co}_{3-x}\text{O}_4$ samples. **d** Fourier-transformed k^3 -weighted Co K-edge X-ray absorption fine structure (EXAFS) spectra of the as-prepared spinel $\text{Li}_x\text{Co}_{3-x}\text{O}_4$ samples.

technique. Figure 2d displays the Fourier-transformed k^3 -weighted Co K-edge EXAFS spectra of the as-prepared samples. The peaks at 1.5 Å and 2.5 Å correspond to Co-O scattering and $\text{Co}_{\text{Oct}}\text{-Co}_{\text{Oct}}$ scattering, respectively. The peak at 3.0 Å corresponds to the $\text{Co}_{\text{Tet}}\text{-Co}_{\text{Oct}}$ scattering. With more lithium substituting cobalt, the intensity of $\text{Co}_{\text{Tet}}\text{-Co}_{\text{Oct}}$ scattering peak steadily decreases, suggesting the gradual absence of tetrahedral cobalt in spinel $\text{Li}_x\text{Co}_{3-x}\text{O}_4$ and therefore implying the occupation of lithium cations in tetrahedral sites. It can be rationally concluded that the as-prepared spinel $\text{Li}_x\text{Co}_{3-x}\text{O}_4$.

Electrochemical analysis of the pristine and fully cycled spinel $\text{Li}_x\text{Co}_{3-x}\text{O}_4$

After confirming the crystal structure and cation occupancy of the as-prepared samples, the electrochemical analysis was conducted. The electrochemical measurements were carried out within a potential window of -1.0–1.62 V (*vs.* RHE) in 1 M KOH, with the catalytic activities being normalized by the surface area of oxides (more details are summarized in Methods). The surface area of oxides was obtained by Brunauer-Emmett-Teller (BET) technique, which has been proved to be suitable for measuring the surface area of metal oxides in powder form²³. The current efficiency of spinel LiCo_2O_4 is $95.4 \pm 2.5\%$ (Supplementary Figure 3), confirming that the measured current mainly originates from OER. Figure 3a summarizes the *iR*-compensated activity of the pristine samples. The non-*iR* compensated results are shown in Supplementary Figure 4. The activity rises with more lithium cations substituting cobalt cations, probably because of the strengthened $\text{Co}_{\text{Oct}}\text{-O}$ covalency²⁴. As the electrochemical cycling continues, the surface and near-surface region of the spinel structure may collapse and evolve into amorphous oxyhydroxides (Fig. 3b). The structural information and OER activity of the fully cycled spinel $\text{Li}_x\text{Co}_{3-x}\text{O}_4$ were analyzed after performing the electrochemical cycling

for 500 times. The XRD and FTIR results of the cycled samples are shown in Supplementary Figure 5, which evidences that the bulk of the samples remains spinel crystal and implies that the reconstruction process mainly occurs on the surface region. To probe the elemental composition of the near surface region after reconstruction, the Co 2p and Li 1s XPS spectra of the cycled samples are recorded (Supplementary Figure 6). As illustrated, no Li 1s spectra can be recorded, suggesting the absence of lithium in the near surface region. Besides, of all the samples, the positions of Co 2p characteristic peaks are quite close to those of CoOOH , which further evidences the formation of surface cobalt oxyhydroxide. Therefore, we believe the active sites after reconstruction should be the CoO_6 units. The O 1s XPS spectra were recorded to investigate the components of various oxygen species in the surface region. As exhibited in Fig. 3c, the relative ratio of lattice oxygen and surface oxyhydroxide becomes much smaller and higher, respectively, with cobalt being gradually substituted by lithium. The numerical ratios can be extracted by calculating the area the characteristic curve covers, which are given in Fig. 3d. The results evidently demonstrate the steady growth of surface oxyhydroxide with more lithium being present inside the spinel lattice, suggesting higher surface reconstruction degree with the increase of lithium cations. The comparison of O 1s XPS spectra between the pristine and cycled samples are shown in Supplementary Figure 7. As demonstrated, compared to the pristine samples, all the cycled ones possess increased ratio of surface oxyhydroxide and decreased ratio of lattice oxygen, suggesting the destruction of spinel structure and the in situ formation of oxyhydroxides. Besides, more lithium incorporation is found to promote the generation of more surface oxyhydroxide, which further evidences the intensified surface reconstruction in high lithium-containing $\text{Li}_x\text{Co}_{3-x}\text{O}_4$. The surface reconstruction can be visually characterized by high-resolution transmission electron

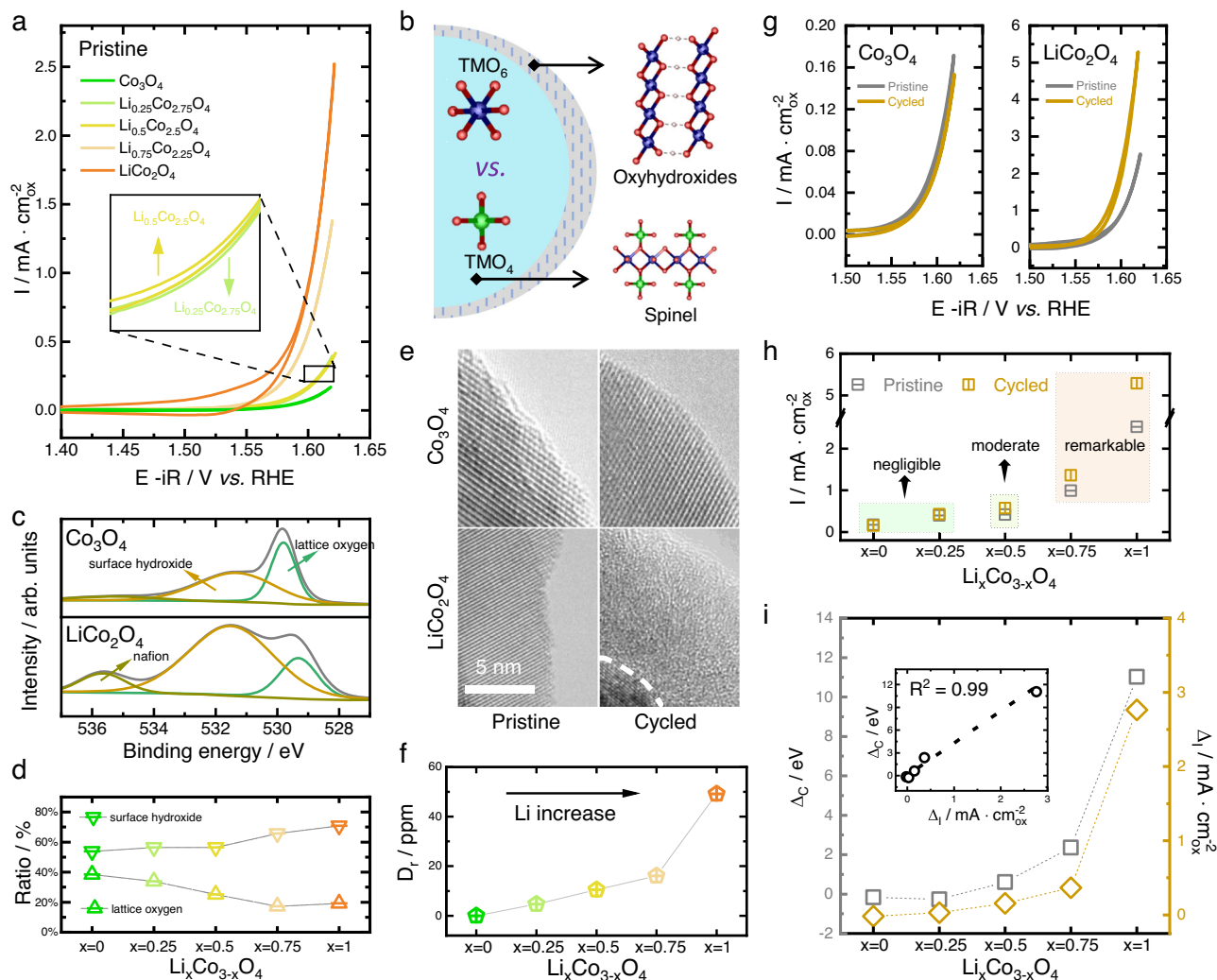


Fig. 3 | Electrochemical analysis of the pristine and fully cycled spinel $\text{Li}_x\text{Co}_{3-x}\text{O}_4$. **a** The cyclic voltammetry (CV) curves of the pristine $\text{Li}_x\text{Co}_{3-x}\text{O}_4$. **b** Schematic of the surface reconstruction of spinel oxides. **c** The O 1s spectra of fully cycled spinel Co_3O_4 and LiCo_2O_4 . **d** The relative ratio of surface oxyhydroxide and lattice oxygen in the fully cycled spinel $\text{Li}_x\text{Co}_{3-x}\text{O}_4$. **e** The high-resolution transmission electron microscopy (HRTEM) images of the pristine and cycled spinel Co_3O_4 and LiCo_2O_4 . **f** The estimated reconstruction degree (D_r) of spinel $\text{Li}_x\text{Co}_{3-x}\text{O}_4$. **g** The CV curve of the pristine and cycled spinel Co_3O_4 and LiCo_2O_4 .

h The experimentally measured current density (@ 1.62 V *vs.* RHE) of the pristine and cycled spinel $\text{Li}_x\text{Co}_{3-x}\text{O}_4$. **i** The plot integrating both the experimentally measured and theoretically calculated reconstruction degree. The current density (@ 1.62 V *vs.* RHE) change (Δ_i) between cycled and pristine spinel $\text{Li}_x\text{Co}_{3-x}\text{O}_4$ is used to represent the experimentally measured reconstruction degree, while the DFT calculated metal-oxygen covalency polarity (the metal-oxygen covalency difference between MO_4 and MO_6 , Δ_c) is used to represent the theoretically predicted reconstruction degree. The insert shows the linear fitting of the two parameters.

microscopy (HRTEM) images. As given in Fig. 3e, the pristine and cycled HRTEM images of Co_3O_4 display smooth and crystallized surface termination, indicating the absence of surface reconstruction. By contrast, remarkable surface amorphization is observed in the cycled HRTEM image of LiCo_2O_4 , reflecting considerable reconstruction at the surface region. The surface reconstruction degree (D_r) can be evaluated by analyzing the volumetric ratio between the reconstructed portion and the totally loaded one, which can be obtained using the following equation (detailed derivation procedures of the equation is summarized in Methods):

$$D_r = \frac{V_{\text{reconstruction}}}{V_{\text{loading}}} = \frac{\frac{c_{\text{Li}} \cdot N_A}{6.94 \cdot x} \cdot V_{\text{mol}}}{\frac{4}{3} \cdot \pi \cdot \left(\sqrt{\frac{m_{\text{loading}} \cdot \text{BET}}{4\pi}} \right)^3} \quad (1)$$

where c_{Li} , N_A , V_{mol} , x , m_{loading} , and *BET* represent the content of Li in the cycled electrolyte, the Avogadro constant, the molecular volume of spinel $\text{Li}_x\text{Co}_{3-x}\text{O}_4$, the stoichiometric number x in spinel $\text{Li}_x\text{Co}_{3-x}\text{O}_4$,

the mass loading, and the BET area of the oxide, respectively. As displayed in Fig. 3f, a noticeable increase of reconstruction degree is observed with the increase of lithium cations in spinel $\text{Li}_x\text{Co}_{3-x}\text{O}_4$. The trend further evidences the intensification of surface reconstruction in high lithium-containing $\text{Li}_x\text{Co}_{3-x}\text{O}_4$.

The change in OER activity gives a more precise evaluation of the surface reconstruction degree. As above-mentioned, all the prepared samples share the same catalytically active centers after reconstruction, i.e., the reconstructed CoO_6 units. This lays the foundation that the activity change between reconstructed catalyst and the pristine one can be convictive for assessing the surface reconstruction degree. The cyclic voltammetry (CV) curves of all the pristine and cycled samples are shown in Supplementary Fig. 8. It is obvious that the introduction of lithium is beneficial for a more apparent catalytic enhancement, as Co_3O_4 exhibits almost unchanged CV curves while LiCo_2O_4 shows dramatic rise after fully cycling (Fig. 3g). It's worth to note that, based on the chronoamperometry results of spinel Co_3O_4 and LiCo_2O_4 (Supplementary Fig. 9), the incorporation of lithium in

spinel structure does not influence the OER durability, as both catalysts exhibit rather stable catalytic performance within 60 operating hours. Figure 3h provides a direct comparison of the current density (@ 1.62 V *vs.* RHE) between the pristine and the cycled one. Similar to that illustrated in Fig. 1d, three distinct regions can be identified. For spinel Co_3O_4 and $\text{Li}_{0.25}\text{Co}_{2.75}\text{O}_4$, the highly overlapped current density suggests negligible surface reconstruction. With more lithium being introduced into spinel $\text{Li}_x\text{Co}_{3-x}\text{O}_4$, the change in current density becomes noticeable. In $\text{Li}_{0.5}\text{Co}_{2.5}\text{O}_4$, the current density of cycled catalyst surpasses that of the spinel pre-catalyst, indicating the surface reconstruction is moderate. In spinel $\text{Li}_{0.75}\text{Co}_{2.25}\text{O}_4$ and LiCo_2O_4 , notable activity improvement can be seen, which signifies remarkable surface reconstruction. It's worth to note that the surface area of samples is expected to increase after reconstruction, which can be evidenced by the measured electrochemically active surface area (ECSA) of the pristine and cycled samples (Supplementary Fig. 10). As exhibited in Supplementary Fig. 10a, the increase of ECSA gets intensified with the increase of lithium in pre-catalyst. This reveals the increased active sites, and therefore demonstrates the higher amorphization degree, in high lithium-containing samples. However, the increase of surface area does not alter the activity trend of the cycled samples (Supplementary Fig. 10b). To directly visualize the reconstruction degree in CV and compare the activities of the pristine and cycled samples within the same context, the current densities of the cycled samples are still normalized by the surface area of the pre-catalysts. By plotting the experimental activity enhancement (the change of current density @ 1.62 V *vs.* RHE, Δ_I) and the calculated metal-oxygen covalency polarity of spinel (the metal-oxygen covalency difference between MO_4 and MO_6 , Δ_C) in the same pattern, a reasonably similar trend is present (Fig. 3i). The fitting between these two parameters shows a R square value of 0.99 (Fig. 3i insert), which strongly demonstrates that the metal-oxygen covalency polarity is reasonable to explain, and therefore can be used to predict, the surface reconstruction ability of spinel oxides. In other words, a structure-reconstruction relationship of spinel oxides can be outlined, i.e., higher metal-oxygen covalency polarity between MO_4 and MO_6 can result in stronger surface reconstruction, and vice versa.

Guidelines for the design of highly active oxyhydroxides from spinel pre-catalysts

Although the profile of surface reconstruction on spinel oxides has been outlined, it remains ambiguous how to maximize the function of surface reconstruction towards optimal reaction performance. This necessitates the understanding of how surface reconstruction contributes to the measured OER activity and what the key factors dominating the activity of oxyhydroxides are. Generally, the activity enhancement of electrochemical reactions can be realized via two aspects, i.e., increasing the number of active sites or increasing the intrinsic activity of active sites³. To figure out how surface reconstruction contributes to the OER activity, electrochemical analysis of cycled $\text{Li}_x\text{Co}_{3-x}\text{O}_4$ is performed. As shown in Fig. 4a, the measured OER activity significantly rises with the increase of amorphization degree, indicating the reaction performance is positively correlated to the degree of surface reconstruction. The intrinsic activities of the generated cobalt oxyhydroxides are compared in Fig. 4b. As shown, the Tafel slopes of the generated cobalt oxyhydroxides are quite close to each other, in which the maximum difference is less than 10 mv dec^{-1} . This suggests all the cobalt oxyhydroxides show similar reaction mechanism and share the same rate-determining step²⁵. The activity per cobalt site is evaluated by calculating the turnover frequency (TOF). As given in Fig. 4b, the TOF values of the five cobalt oxyhydroxides are within the range of 0.01 s^{-1} to 0.02 s^{-1} . Considering the observation that TOF can range across many orders of magnitude, these values indicate the intrinsic activity of each cobalt site in the five oxyhydroxides is almost identical to each other²⁵. Therefore, we can

rationally deduce that, for pre-catalysts with the same metal cation, an increased reconstruction ability does not alter the intrinsic catalytic activity of the active sites in the in situ generated amorphous oxyhydroxide, but contributes to the enhanced activity by increasing the number of available active sites.

The demonstrated structure-reconstruction relationship also allows us to design spinel pre-catalysts with the same reconstruction ability, based on which we can in situ generate oxyhydroxides with the same amorphization degree to investigate the influence of cation type and ratio on the OER activity of oxyhydroxides. Specifically, the reconstruction ability of spinel $\text{Zn}[\text{Al}_{1.5}\text{M}_{0.5}]\text{O}_4$ ($\text{M} = \text{FeCo}, \text{FeNi}, \text{FeMn}, \text{CoNi}, \text{CoMn}, \text{and NiMn}$) were screened to search for spinel pre-catalysts with the same reconstruction ability. The cations of iron, cobalt, nickel, and manganese were studied because they are earth-abundant and therefore exhibit cost advantage for potential commercial usage. The screening results are summarized in Fig. 4c. It can be seen that, in zinc aluminum spinel substrate, the introduction of octahedral nickel cation and manganese cation generally results in higher and lower reconstruction ability, respectively. The Δ_C value of 3.5 eV is chosen as a reference line to select spinel pre-catalysts with the same reconstruction ability. The Δ_C value of 3.5 eV is chosen because it guarantees a high-level reconstruction ability of spinel pre-catalyst and can incorporate sufficient screened samples with the same reconstruction ability to design control experiment for the catalytic investigations on the in situ generated oxyhydroxides. Specifically, spinel $\text{Zn}[\text{Al}_{1.5}\text{Fe}_{0.125}\text{Co}_{0.375}]\text{O}_4$, $\text{Zn}[\text{Al}_{1.5}\text{Fe}_{0.25}\text{Co}_{0.25}]\text{O}_4$, $\text{Zn}[\text{Al}_{1.5}\text{Fe}_{0.375}\text{Co}_{0.125}]\text{O}_4$, $\text{Zn}[\text{Al}_{1.5}\text{Fe}_{0.375}\text{Ni}_{0.125}]\text{O}_4$, and $\text{Zn}[\text{Al}_{1.5}\text{Co}_{0.375}\text{Ni}_{0.125}]\text{O}_4$ are selected to serve as pre-catalysts to generate the bimetallic oxyhydroxides. Subsequent experiments were conducted to synthesize the selected spinel pre-catalysts. The XRD characterization confirmed the spinel crystal of the prepared samples (Supplementary Figure 12). Electrochemical measurements were thereafter performed to in situ generate the corresponding amorphous oxyhydroxides. To guarantee a complete reconstruction, the measurements were conducted for at least 500 cycles until a stable electrochemical curve appears. The TEM images of the samples after reaction are shown in Supplementary Figure 13, which evidence the generation of amorphous layers and nearly the same amorphization degree. Besides, the point scan results (Supplementary Figure 14) confirmed the metal-metal ratio in the amorphous layers is about the same as that in the spinel pre-catalysts.

The electrochemical activity of the generated oxyhydroxides were analyzed and shown in Fig. 4d. The results demonstrate the activity of oxyhydroxides can be largely influenced by the cation type and cation ratio. The comparison between $\text{Ni}_{0.25}\text{Fe}_{0.75}\text{OOH}$ and $\text{Ni}_{0.25}\text{Co}_{0.75}\text{OOH}$ suggests that the reactivity of iron cation in oxyhydroxide is higher than that of cobalt cation, consistent with the conclusion reported in other reports^{11,25}. The comparison between iron-cobalt oxyhydroxides with different Fe/Co ratio, however, shows a trend that the activity increases with the increase of cobalt ratio in oxyhydroxides. This is a phenomenon that inevitably occurs during OER, in which small amount of iron (normally less than 40%) can significantly raise the activity of cobalt-based oxyhydroxides^{12,25-28}. There are two possible reasons. One is that the CoO_6 units serve as a conductive and chemically stable host for iron species, which are intrinsically very active but are electrically insulating^{25,28,29}. The other is that the formation of high-valent iron species (normally refers to Fe^{4+}), serving either as direct catalytic centers or as redox activators for cobalt cations, is the key for the superior activity^{27,28}. To identify the dominant factor for the iron-cobalt oxyhydroxides generated from spinel pre-catalysts, we further investigated the charge transport ability and cation oxidation state.

As elucidated elsewhere, the oxygen hole density is an effective index to estimate the charge transport ability within the transition metal oxides (TMOs), where a higher hole density suggests a higher charge transport ability³⁰⁻³². The calculated oxygen hole density is presented in Fig. 4e. For FeOOH , only traceable hole density (0.002 μ_B)

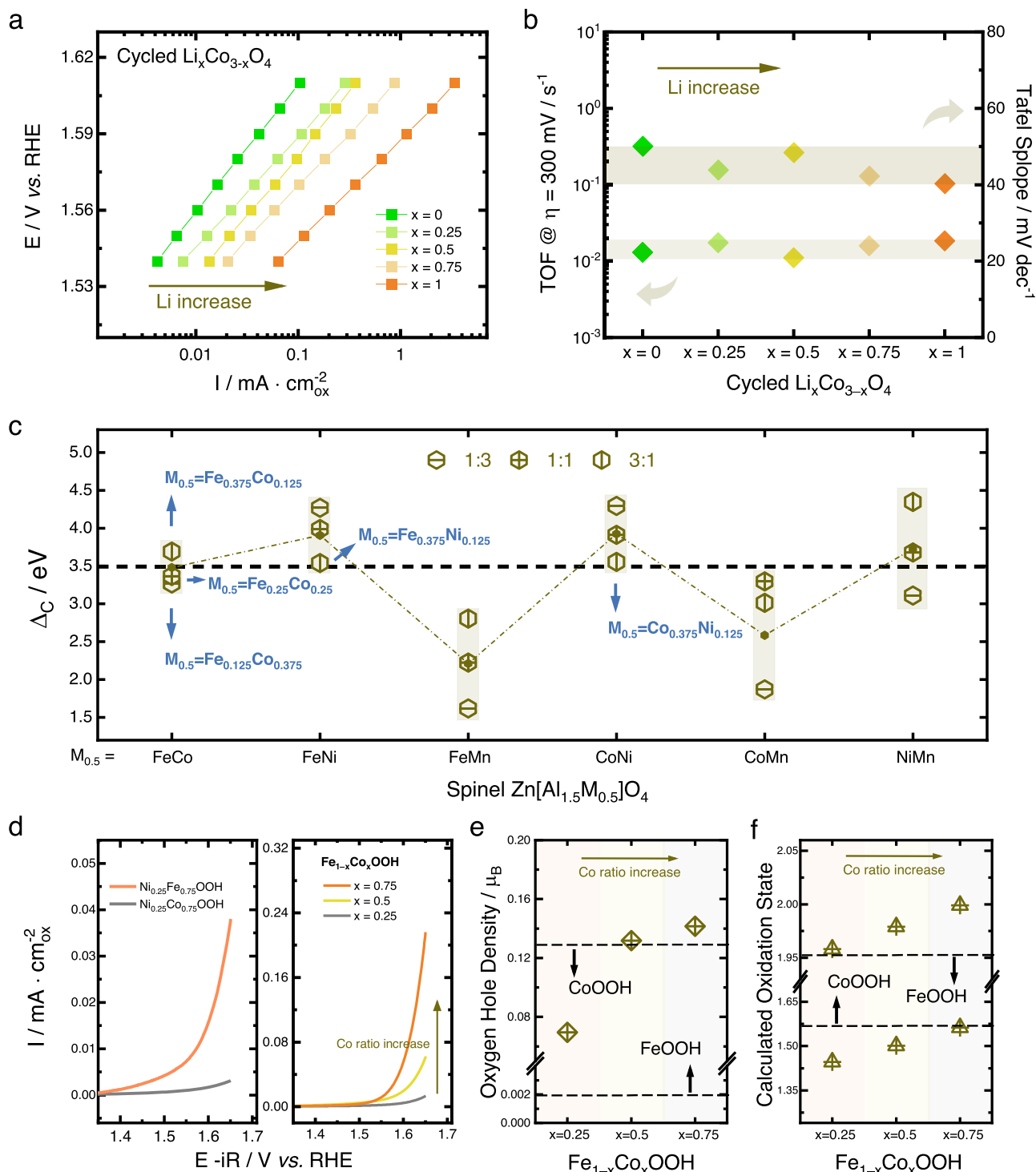


Fig. 4 | Investigation of the reconstructed oxyhydroxides from spinel pre-catalysts. **a** The Tafel plots of the cycled spinel $\text{Li}_x\text{Co}_{3-x}\text{O}_4$. **b** The Tafel slope and turnover frequency (TOF) of cycled spinel $\text{Li}_x\text{Co}_{3-x}\text{O}_4$. **c** The calculated structural polarity of spinel $\text{Zn}[\text{Al}_{1.5}\text{M}_{0.5}]\text{O}_4$ ($\text{M} = \text{FeCo}, \text{FeNi}, \text{FeMn}, \text{CoNi}, \text{CoMn}, \text{and NiMn}$). For each bimetallic combination, three metal-metal ratios, i.e., 1:3, 1:1, and 3:1, are calculated. **d** The cyclic voltammetry (CV) curves of $\text{Ni}_{0.25}\text{Fe}_{0.75}\text{OOH}$, $\text{Ni}_{0.25}\text{Co}_{0.75}\text{OOH}$, and $\text{Fe}_{1-x}\text{Co}_x\text{OOH}$ ($x = 0.25, 0.5, \text{and } 0.75$). The oxyhydroxides are in situ generated from spinel pre-catalyst $\text{Zn}[\text{Al}_{1.5}\text{Ni}_{0.125}\text{Fe}_{0.375}]\text{O}_4$.

$\text{Zn}[\text{Al}_{1.5}\text{Ni}_{0.125}\text{Co}_{0.375}]\text{O}_4$, $\text{Zn}[\text{Al}_{1.5}\text{Fe}_{0.375}\text{Co}_{0.125}]\text{O}_4$, $\text{Zn}[\text{Al}_{1.5}\text{Fe}_{0.25}\text{Co}_{0.25}]\text{O}_4$, and $\text{Zn}[\text{Al}_{1.5}\text{Fe}_{0.125}\text{Co}_{0.375}]\text{O}_4$. The curves are capacitance-corrected by averaging the forward and backward sweeps. **e** The calculated oxygen hole density (μB) of $\text{Fe}_{1-x}\text{Co}_x\text{OOH}$ ($x = 0.25, 0.5, \text{and } 0.75$). The oxygen hole density of FeOOH and CoOOH is also shown for reference. **f** The calculated oxidation state of cobalt and iron cations in $\text{Fe}_{1-x}\text{Co}_x\text{OOH}$ ($x = 0.25, 0.5, \text{and } 0.75$). The dashed lines represent the oxidation state of iron cation in FeOOH and that of cobalt cation in CoOOH .

is observed, indicating an insulating nature. When 25% cobalt cations are introduced ($\text{Fe}_{0.75}\text{Co}_{0.25}\text{OOH}$), the oxygen hole density dramatically increases and reaches $0.07 \mu\text{B}$, suggesting a significant increase of charge transport ability. When the cobalt ratio further increases to 50%

($\text{Fe}_{0.5}\text{Co}_{0.5}\text{OOH}$), the oxygen hole density undergoes another dramatic increase to reach $0.13 \mu\text{B}$. With further increase of cobalt ratio to 75%, the oxygen hole density of $\text{Fe}_{0.25}\text{Co}_{0.75}\text{OOH}$ is $0.14 \mu\text{B}$ and is close to that of $\text{Fe}_{0.5}\text{Co}_{0.5}\text{OOH}$, which implies that the charge transport

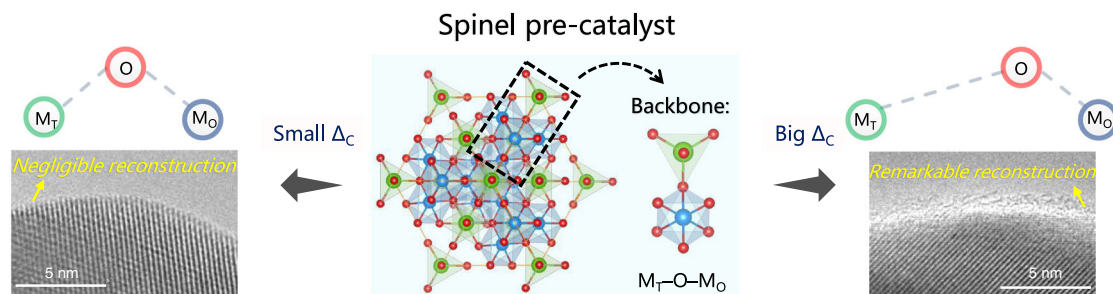


Fig. 5 | Schematic of the structure-reconstruction relationship for spinel pre-catalyst during water oxidation.

ability within iron-cobalt oxyhydroxides may not undergo further increment with additional incorporation of cobalt cations. Noting that the oxygen hole density on CoOOH is $0.129 \mu_{\text{B}}$, the values of $0.13 \mu_{\text{B}}$ on $\text{Fe}_{0.5}\text{Co}_{0.5}\text{OOH}$ and $0.14 \mu_{\text{B}}$ on $\text{Fe}_{0.25}\text{Co}_{0.75}\text{OOH}$ indicate that their charge transport ability has already reached the level at which it is no longer the bottleneck of the reaction. Therefore, we may conclude that the poor charge transport ability is the main catalytical drawback of iron-cobalt oxyhydroxide when the cobalt ratio is less than 50% (iron ratio higher than 50%).

The calculated cation oxidation states are shown in Fig. 4f. The two dashed lines represent the oxidation state of cobalt and iron in CoOOH and FeOOH , respectively. The trend evidences a gradual increase of iron oxidation state with the increase of cobalt ratio, which implies the presence of high-valent iron cations in low-iron-containing iron-cobalt oxyhydroxides. Considering the charge transport ability is no longer a catalytical drawback for iron-cobalt oxyhydroxides with cobalt ratio more than 50%, the activity enhancement with additional cobalt incorporation may attribute to the increased iron oxidation state that facilitates an in situ generation of high-valent iron cations under OER potential. Therefore, the design of highly active and cost-effective oxyhydroxides from spinel pre-catalysts should consider two aspects: (i) the high reconstruction ability that guarantees the availability of more active sites and (ii) the incorporation of conductive and high-valent iron cations that guarantees high intrinsic activity of the active sites.

Potential of surface reconstruction ability of spinel oxides

As demonstrated above, the structural origin of surface reconstruction on spinel oxides has been identified and a criterion evaluating the surface reconstruction ability of spinel oxides is unveiled (Fig. 5). To design spinel oxide with high reconstruction ability for the generation of more available active sites, strategies should be made to weaken the metal-oxygen covalency of MO_4 and strengthen that of MO_6 . By contrast, if a spinel pre-catalyst is believed to hold remarkable intrinsic activity for OER, approaches are therefore needed to balance the metal-oxygen covalency between MO_4 and MO_6 to guarantee a stable in situ spinel crystal frame for long reaction durability.

Employing the computational database established in our previous work¹⁷, a computational high-throughput figure can be plotted to evaluate the reconstruction ability of spinel oxides, which is shown in Fig. 6. The x -axis presents a parameter that can be used to evaluate the possibility of existence of spinel oxides, which is demonstrated in our previous study³³. According to our findings, the value of $O p$ states relative to $M_o d$ states of phase-pure spinel oxides is normally below 1 eV ³³. It can be seen that most of the data points are located within the phase-pure region, ensuring the effectiveness of using this database to screen the properties of spinel oxides. As labeled, spinel LiCo_2O_4 exhibits tremendous potential for in situ surface reconstruction, indicating it can be used as an ideal pre-catalyst with high reconstruction ability to generate cobalt-oxyhydroxide-host for active cation (such as iron) substitution. Besides, it's worth to note that the Δ_C value of spinel LiMn_2O_4 is only -1.373 eV , which indicates strong resistivity towards

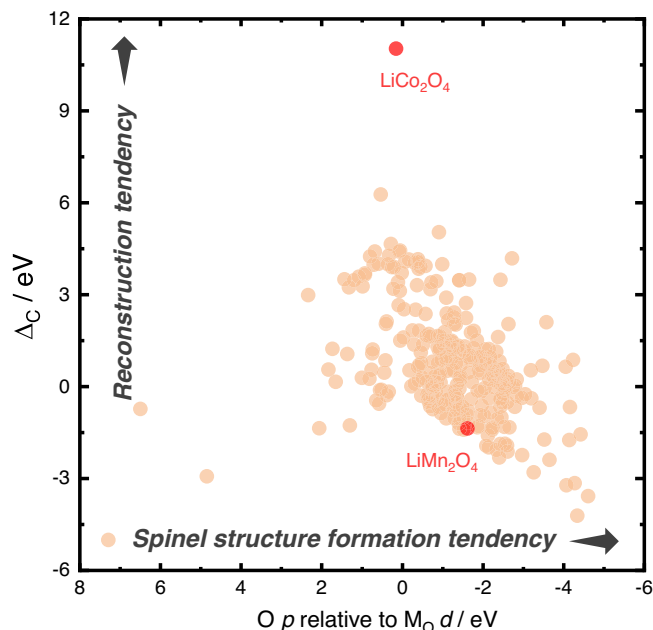


Fig. 6 | Surface reconstruction ability of various spinel oxides. High-throughput plot showing the reconstruction ability of various spinel oxides. The data points are taken from ref. 17 The x -axis is a parameter that can be used to evaluate the structure formation tendency of spinel oxides, which was proposed in ref. 33.

reconstruction. This explains why lithium cannot leach out from LiMn_2O_4 lattice and therefore the spinel structure remains almost unchanged during OER. The overall Δ_C range of spinel oxides is from -6 eV to 12 eV , which demonstrates a huge structural flexibility to manipulate the reconstruction degree. Therefore, we can conclude that spinel oxides are a big family of transition metal oxides with high flexibility to serve as pre-catalysts for electrochemical water oxidation.

In summary, combining computational and experimental analysis, we have pinpointed and demonstrated the structure-reconstruction relationship of surface reconstruction on spinel oxides. The metal-oxygen covalency polarity of the $\text{M}_T\text{-O-M}_O$ backbone is proved to be the structural origin that triggers surface reconstruction, in which higher polarity corresponds to greater degree of reconstruction. With the established structure-reconstruction relationship, the reconstruction ability of spinel pre-catalysts can be precisely predicted and subtly manipulated. Besides, by conducting mechanistic study on a series of oxyhydroxides generated from spinel pre-catalysts, we have showcased how surface reconstruction contributes to OER activity and how activity of the generated oxyhydroxides evolves with the change of cation type and cation ratio. Our work unveils the key fundamentals of surface reconstruction on spinel oxides and provides firm theoretical foundations for the spinel pre-catalyst design. The research scenario

for studying the surface reconstruction may also be extended to other types of TMOs.

Methods

Density functional theory (DFT) calculations

The DFT calculations were performed by the Vienna Ab-initio Simulation Package^{34,35} (VASP), employing the Projected Augmented Wave³⁶ (PAW) method. The exchange and correlation effects were described by using the Perdew-Burke-Ernzerhof³⁷ (PBE) functional. The cutoff energy was set to be 450 eV in all the cases. The GGA + U calculations were performed using the model proposed by Dudarev et al.³⁸. The effective Hubbard U values were set to be 4.5 eV, 4.7 eV, 3.3 eV, 4 eV, 6.4 eV, and 4 eV for tetrahedral Co, tetrahedral Zn, octahedral Co, octahedral Fe, octahedral Ni, and octahedral Mn, respectively. The Monkhorst-Pack grids were set to be $6 \times 6 \times 6$ and $9 \times 9 \times 9$ for performing the structural optimization and density of states calculations, respectively. The conventional standard cell of spinel oxide is employed in this work, in which 8 tetrahedral cations, 16 octahedral cations and 32 oxygen anions are contained. During the model construction, all the lithium cations in the lithium-containing spinels are placed in the tetrahedral sites, as both theoretical³⁹ and experimental^{40,41} proofs have demonstrated the energetic preference of lithium in tetrahedral sites. The different placement of cobalt and lithium cations in tetrahedral sites does not affect the derived band center of ions since no M_T-O-M_T bond exists in spinel structure.

The vacancy formation energy was calculated as the energy difference between the vacant spinel together with an oxygen atom and the intact spinel structure, which was defined as

$$E_{vac-O} = E_{vacant-bulk} + E_{oxygen} - E_{intact-bulk} \quad (2)$$

where $E_{vacant-bulk}$, E_{oxygen} , and $E_{intact-bulk}$ represent the electronic energy of the spinel with one bulk oxygen vacancy, the chemical potential of one oxygen atom referenced to gaseous oxygen molecule, and the electronic energy of the intact spinel, respectively⁴². Under this definition, a lower value of bulk oxygen formation energy suggests an easier case for generating an oxygen vacancy.

The surface transformation energy from spinel to layered oxide was calculated as the energy difference (per surface area) between the reconstructed species and the intact spinel surface, which was defined as

$$E_{spinel\ to\ CoOO} = \frac{E_{spinel-slab} - n_1 E_{CoOO} - n_2 Co - n_3 Li}{S^2} \quad (3)$$

where $E_{spinel-slab}$, E_{CoOO} , n_1 , n_2 , n_3 , and S represent the electronic energy of the spinel slab model, the layered CoOO species, the number of reconstructed CoOO species, the number of cobalt cations in the tetrahedral sites of spinel slab, the number of lithium cations in the tetrahedral sites, and the surface area of the spinel slab, respectively. Under this definition, a lower value of surface transformation energy suggests an easier transformation from spinel structure to layered structure.

Synthesis of the spinel pre-catalysts

The spinel pre-catalysts were synthesized by a modified conventional sol-gel combustion method. Metal acetates $Co(CH_3COO)_2 \cdot 4H_2O$ (99.999% trace metals basis, Sigma-Aldrich), $Zn(CH_3COO)_2 \cdot 2H_2O$, $Mn(CH_3COO)_2 \cdot 4H_2O$, $Ni(CH_3COO)_2 \cdot 4H_2O$, $Fe(NO_3)_3 \cdot 9H_2O$ (Sigma-Aldrich), and $LiNO_3$ (Sigma-Aldrich) with a specific molar ratio were first mixed in diluted nitric acid solution through vigorous stirring. Citric acid (ACS reagent, $\geq 99.5\%$, Sigma-Aldrich) acting as chelating agent, was the added in the mixture. Under the condition of constant stirring at 90 °C for several hours, the mixture solution converts into viscous gel. The gel was then decomposed in air at 170 °C (with a heating rate of

10 °C min⁻¹ to 170 °C) for 12 hours to remove the remaining water and ground thoroughly. After applying a further heat treatment in air at 400 °C for six hours, phase pure spinel oxide powders were obtained.

Procedures of electrochemical analysis

The OER analysis was operated in a three-electrode cell with a working electrode of glassy carbon flake (effective electrode area: 0.196 cm²), a counter electrode of platinum foil, and a Hg/HgO reference electrode filled with 1M KOH solution. The 1M KOH solution was prepared by using electronic grade KOH (purity 99.999%, Aladdin), which excludes the Fe contamination issue⁴³. The catalyst electrode was fabricated by the recipe drop-castes method. The catalysts were mixed with acetylene black (AB) at a mass ration of 5:1, then dispersed in isopropanol/water ($v/v = 1:4$) solvent followed by the addition of Na⁺-exchanged Nafion as the binder. The mixtures were ultrasonicated for 30 min to reach homogeneous ink. The concentration of oxides in ink is 5 mg/ml, and AB is 1 mg/ml. Before drop-casting, the glassy carbon electrodes were polished to a mirror with $\alpha-Al_2O_3$ (50 nm) and washed by IPA and water to clean up completely. Finally, the as-prepared ink (10 μ l) was dropped onto glassy carbon electrodes to reach a loading mass of 50 μ g_{ox} cm⁻² and the electrodes were dried overnight at room temperature. Cyclic voltammograms (CVs), linear sweep voltammetry (LSV) and chronoamperometry (CA) were performed in O₂-saturated 1M KOH by using Bio-logic SP 150 potentiostat. The potential range was set from 0.90 V to 1.62 V (*vs.* RHE). The scan rate was kept at 10 mV s⁻¹. All potentials were converted to RHE scale with iR correction according to

$$E(\text{vs. RHE}) = E(\text{vs. Hg/HgO}) + 0.059 \cdot pH + 0.098. \quad (4)$$

The pH value of the electrolyte was obtained from pH meter measurement by using Orion StarTM A121 portable pH meter (Thermo Fisher Scientific), from which pH values of 14.00 ± 0.05 were measured in this work. The internal resistance was determined right after the CV measurements by electrochemical impedance spectroscopy (EIS). The EIS measurement was conducted by collecting the AC impedance spectra from 200 kHz to 1 Hz with a voltage perturbation of 10 mV versus a constant potential. The internal resistance was the real part of the impedance where the imaginary part of the impedance was zero in the Nyquist plot. The measured internal resistance is $5.00 \pm 0.05 \Omega$ in this work. The OER polarization curves were then corrected to obtain the iR-free potential ($E - iR$) of the working electrode.

Turnover frequency (TOF) calculations

In this work, the TOFs were calculated via the redox method, which is commonly employed in the system of oxyhydroxides. Specifically, the TOF calculation is based on the following equation:

$$TOF = \frac{I_{ox} \times A_{ox}}{4 \times e \times N} = \frac{E}{4 \times e \times N} \quad (5)$$

where I_{ox} , A_{ox} , E , e , and N represent the BET normalized current density at the overpotential of 300 mV, the oxide surface area measured by BET, the measured current on the electrode, the charge of a single electron, and the number of cobalt atoms in the electrode. The number of cobalt atoms (N) is estimated by the integration of Co redox peak at ≈ 1.15 V *vs.* RHE (assuming a one-electron process of Co^{2+}/Co^{3+}).

Derivation of surface reconstruction degree (D_r)

The surface reconstruction degree was evaluated on the basis that the loaded catalysts can be considered as a sphere model. With the measurement of Brunauer-Emmett-Teller (BET), the total surface area of the loaded pre-catalyst can be obtained by $m_{loading} \cdot BET$. So the

following equation can be obtained

$$m_{\text{loading}} \cdot \text{BET} = 4\pi(R_{\text{loading}})^2. \quad (6)$$

Based on above equation, the radius of the loaded pre-catalyst (R_{load}) can be obtained as

$$R_{\text{loading}} = \sqrt{\frac{m_{\text{loading}} \cdot \text{BET}}{4\pi}}. \quad (7)$$

The volume of the loaded pre-catalyst can therefore be evaluated as

$$V_{\text{loading}} = \frac{4}{3} \cdot \pi \cdot \left(\sqrt{\frac{m_{\text{loading}} \cdot \text{BET}}{4\pi}} \right)^3. \quad (8)$$

The reconstructed part can be evaluated by the solvated lithium cations in the electrolyte. By conducting inductively coupled plasma (ICP) analysis, the content of the solvated lithium cations (c_{Li} , with the unit of g) can be obtained. The mole of lithium cations can then be obtained as $\frac{c_{\text{Li}}}{6.94}$, where 6.94 ($g \text{ mol}^{-1}$) is the molar mass of lithium. The number of lithium cations in the solution can be evaluated as $\frac{c_{\text{Li}} \cdot N_A}{6.94}$, where N_A is the Avogadro constant. The number of the solvated spinel molecule can be evaluated as $\frac{c_{\text{Li}} \cdot N_A}{6.94 \cdot x}$, where x is the stoichiometric number in spinel $\text{Li}_x\text{Co}_{3-x}\text{O}_4$. The reconstructed volume of spinel pre-catalyst can therefore be evaluated as

$$V_{\text{reconstruction}} = \frac{c_{\text{Li}} \cdot N_A}{6.94 \cdot x} \cdot V_{\text{mol}}. \quad (9)$$

where V_{mol} is the volume of one spinel molecule obtained from DFT calculations. Based on above derivations, the reconstruction degree (D_r) can be evaluated as

$$D_r = \frac{V_{\text{reconstruction}}}{V_{\text{loading}}} = \frac{\frac{c_{\text{Li}} \cdot N_A}{6.94 \cdot x} \cdot V_{\text{mol}}}{\frac{4}{3} \cdot \pi \cdot \left(\sqrt{\frac{m_{\text{loading}} \cdot \text{BET}}{4\pi}} \right)^3}. \quad (10)$$

Materials characterization

The X-ray diffraction (XRD) of spinel oxides were carried out on Bruker D8 diffractometer at a scanning rate of 2° min^{-1} , under Cu-K α radiation ($\lambda = 1.5418 \text{ \AA}$). The X-ray photoelectron spectroscopy (XPS) measurements were performed using PHI-5400 equipment with Al K α beam source (250 W) and a position-sensitive detector (PSD) was used to determine the surface composition of the materials. Fourier transform infrared spectroscopy (FTIR) data were recorded using FTIR PerkinElmer Spectrum. The inductively coupled plasma-optical emission spectrometry (ICP-OES) characterizations were performed using Agilent 720 with a detection limit of 0.02 ppm. The sample powders were weighed (accuracy 0.1 mg) and put in a dry beaker. Then 4 mL of aqua regia solution was added into the beaker and heated at 80°C until the powders were fully dissolved. The solution was allowed to cool naturally to room temperature in fume hood before being transferred into a 25 mL volumetric flask. Deionized (DI) water was added to dilute the solution to 25 mL and was shaken thoroughly for ICP-OES testing. The X-ray absorption near edge spectroscopy (XANES) and extended X-ray absorption fine structure (EXAFS) experiments were conducted in transmission mode at beamline XAFCA of the Singapore Synchrotron Light Source⁴⁴. The data reduction and data analysis were performed with the Athena, Artemis and IFEFFIT software packages. The EXAFS data were extracted from the measured absorption spectra using standard procedures. A cubic-spline-fit procedure was used to determine the post-edge background with a subsequent subtraction. Normalization was performed by dividing the data by the height of the absorption edge at 50 eV. The results of Brunauer-Emmett-Teller (BET)

measurements are summarized in Supplementary Figure 2 and Supplementary Table 3.

Data availability

The data supporting the findings of this study are available within the article and its Supplementary Information. Additional data are available from the corresponding author upon reasonable request.

References

- Staffell, I. et al. The role of hydrogen and fuel cells in the global energy system. *Energy Environ. Sci.* **12**, 463–491 (2019).
- Stamenkovic, V. R., Strmcnik, D., Lopes, P. P. & Markovic, N. M. Energy and fuels from electrochemical interfaces. *Nat. Mater.* **16**, 57–69 (2017).
- Seh, Z. W. et al. Combining theory and experiment in electrocatalysis: Insights into materials design. *Science* **355**, eaad4998 (2017).
- Nørskov, J. K., Abild-Pedersen, F., Studt, F. & Bligaard, T. Density functional theory in surface chemistry and catalysis. *Proc. Natl Acad. Sci. USA* **108**, 937–943 (2011).
- Nørskov, J. K., Bligaard, T., Rossmeisl, J. & Christensen, C. H. Towards the computational design of solid catalysts. *Nat. Chem.* **1**, 37–46 (2009).
- Seitz, L. C. et al. A highly active and stable IrO $_x$ /SrIrO $_3$ catalyst for the oxygen evolution reaction. *Science* **353**, 1011–1014 (2016).
- Suntivich, J., May, K. J., Gasteiger, H. A., Goodenough, J. B. & Shao-Horn, Y. A perovskite oxide optimized for oxygen evolution catalysis from molecular orbital principles. *Science* **334**, 1383–1385 (2011).
- Gao, L., Cui, X., Sewell, C. D., Li, J. & Lin, Z. Recent advances in activating surface reconstruction for the high-efficiency oxygen evolution reaction. *Chem. Soc. Rev.* **50**, 8428–8469 (2021).
- Liu, X. et al. Comprehensive understandings into complete reconstruction of precatalysts: synthesis, applications, and characterizations. *Adv. Mater.* **33**, 2007344 (2021).
- Fabbri, E. et al. Dynamic surface self-reconstruction is the key of highly active perovskite nano-electrocatalysts for water splitting. *Nat. Mater.* **16**, 925–931 (2017).
- Burke, M. S., Enman, L. J., Batchellor, A. S., Zou, S. & Boettcher, S. W. Oxygen evolution reaction electrocatalysis on transition metal oxides and (oxy) hydroxides: activity trends and design principles. *Chem. Mater.* **27**, 7549–7558 (2015).
- Dionigi, F. et al. Intrinsic electrocatalytic activity for oxygen evolution of crystalline 3d-transition metal layered double hydroxides. *Angew. Chem.* **133**, 14567–14578 (2021).
- Chen, Y. et al. Lattice site-dependent metal leaching in perovskites toward a honeycomb-like water oxidation catalyst. *Sci. Adv.* **7**, eabk1788 (2021).
- Wang, J. et al. Redirecting dynamic surface restructuring of a layered transition metal oxide catalyst for superior water oxidation. *Nat. Catal.* **4**, 212–222 (2021).
- Köhler, L., Abrishami, M., Ebrahimzadeh, Roddatis, V., Geppert, J. & Risch, M. Mechanistic parameters of electrocatalytic water oxidation on LiMn $_2$ O $_4$ in comparison to natural photosynthesis. *ChemSusChem* **10**, 4479–4490 (2017).
- Wei, C. et al. Cations in octahedral sites: a descriptor for oxygen electrocatalysis on transition-metal spinels. *Adv. Mater.* **29**, 1606800 (2017).
- Sun, Y. et al. Covalency competition dominates the water oxidation structure–activity relationship on spinel oxides. *Nat. Catal.* **3**, 554–563 (2020).
- Tronel, F. et al. New spinel cobalt oxides, potential conductive additives for the positive electrode of Ni–MH batteries. *Chem. Mater.* **18**, 5840–5851 (2006).
- Xu, L. et al. Plasma-engraved Co $_3$ O $_4$ nanosheets with oxygen vacancies and high surface area for the oxygen evolution reaction. *Angew. Chem.* **128**, 5363–5367 (2016).

20. Barreca, D. et al. Composition and microstructure of cobalt oxide thin films obtained from a novel cobalt (II) precursor by chemical vapor deposition. *Chem. Mater.* **13**, 588–593 (2001).
21. Yang, W.-D., Hsieh, C.-Y., Chuang, H.-J. & Chen, Y.-S. Preparation and characterization of nanometric-sized LiCoO₂ cathode materials for lithium batteries by a novel sol–gel method. *Ceram. Int.* **36**, 135–140 (2010).
22. Mouhib, Y., Belaiche, M., Ferdi, C. A., Lacham, M. & Elacham, A. New technique for elaboration and characterization of a high voltage spinel LiCo₂O₄ cathode and theoretical investigation. *N. J. Chem.* **44**, 2538–2546 (2020).
23. Wei, C. et al. Approaches for measuring the surface areas of metal oxide electrocatalysts for determining their intrinsic electrocatalytic activity. *Chem. Soc. Rev.* **48**, 2518–2534 (2019).
24. Zhou, Y. et al. Enlarged Co–O covalency in octahedral sites leading to highly efficient spinel oxides for oxygen evolution reaction. *Adv. Mater.* **30**, 1802912 (2018).
25. Burke, M. S., Kast, M. G., Trotochaud, L., Smith, A. M. & Boettcher, S. W. Cobalt–iron (oxy) hydroxide oxygen evolution electrocatalysts: the role of structure and composition on activity, stability, and mechanism. *J. Am. Chem. Soc.* **137**, 3638–3648 (2015).
26. Enman, L. J. et al. Operando x-ray absorption spectroscopy shows iron oxidation is concurrent with oxygen evolution in cobalt–iron (oxy) hydroxide electrocatalysts. *Angew. Chem.* **130**, 13022–13026 (2018).
27. Li, N., Hadt, R. G., Hayes, D., Chen, L. X. & Nocera, D. G. Detection of high-valent iron species in alloyed oxidic cobaltates for catalysing the oxygen evolution reaction. *Nat. Commun.* **12**, 1–6 (2021).
28. Lee, S., Moysiadou, A., Chu, Y.-C., Chen, H. M. & Hu, X. Tracking high-valent surface iron species in the oxygen evolution reaction on cobalt iron (oxy) hydroxides. *Energy Environ. Sci.* <https://doi.org/10.1039/D1EE02999A> (2022).
29. Zhang, T., Nellist, M. R., Enman, L. J., Xiang, J. & Boettcher, S. W. Modes of Fe incorporation in Co–Fe (Oxy) hydroxide oxygen evolution electrocatalysts. *ChemSusChem* **12**, 2015–2021 (2019).
30. Sun, Y. et al. Spin-related electron transfer and orbital interactions in oxygen electrocatalysis. *Adv. Mater.* **32**, 2003297 (2020).
31. Zhang, L., Cheruvathur, A., Biz, C., Fianchini, M. & Gracia, J. Ferromagnetic ligand holes in cobalt perovskite electrocatalysts as an essential factor for high activity towards oxygen evolution. *Phys. Chem. Chem. Phys.* **21**, 2977–2983 (2019).
32. Ju, H., Sohn, H.-C. & Krishnan, K. M. Evidence for O₂ p hole-driven conductivity in La_{1-x}Sr_xMnO₃ (0 ≤ x ≤ 0.7) and La_{0.7}Sr_{0.3}MnO₃ thin films. *Phys. Rev. Lett.* **79**, 3230 (1997).
33. Duan, Y. et al. Mastering surface reconstruction of metastable spinel oxides for better water oxidation. *Adv. Mater.* **31**, 1807898 (2019).
34. Kresse, G. & Hafner, J. Ab initio molecular-dynamics simulation of the liquid-metal–amorphous-semiconductor transition in germanium. *Phys. Rev. B* **49**, 14251 (1994).
35. Kresse, G. & Furthmüller, J. Efficient iterative schemes for ab initio total-energy calculations using a plane-wave basis set. *Phys. Rev. B* **54**, 11169 (1996).
36. Blöchl, P. E. Projector augmented-wave method. *Phys. Rev. B* **50**, 17953 (1994).
37. Perdew, J. P., Burke, K. & Ernzerhof, M. Generalized gradient approximation made simple. *Phys. Rev. Lett.* **77**, 3865 (1996).
38. Dudarev, S. L., Botton, G. A., Savrasov, S. Y., Humphreys, C. & Sutton, A. P. Electron-energy-loss spectra and the structural stability of nickel oxide: An LSDA+U study. *Phys. Rev. B* **57**, 1505 (1998).
39. Van der Ven, A. & Ceder, G. Electrochemical properties of spinel Li₂CoO₂: A first-principles investigation. *Phys. Rev. B* **59**, 742 (1999).
40. Sun, S. et al. Shifting oxygen charge towards octahedral metal: a way to promote water oxidation on cobalt spinel oxides. *Angew. Chem.* **131**, 6103–6108 (2019).
41. Choi, S. & Manthiram, A. Chemical synthesis and properties of spinel Li_{1-x}Co₂O_{4-δ}. *J. Solid State Chem.* **164**, 332–338 (2002).
42. Lee, Y.-L., Kleis, J., Rossmeisl, J., Shao-Horn, Y. & Morgan, D. Prediction of solid oxide fuel cell cathode activity with first-principles descriptors. *Energy Environ. Sci.* **4**, 3966–3970 (2011).
43. Ren, X. et al. Constructing an adaptive heterojunction as a highly active catalyst for the oxygen evolution reaction. *Adv. Mater.* **32**, 2001292 (2020).
44. Du, Y. et al. XAFCA: a new XAFS beamline for catalysis research. *J. Synchrotron Radiat.* **22**, 839–843 (2015).

Acknowledgements

This work was supported by Singapore Ministry of Education Tier 2 Grant (MOE-T2EP10220-0001) and the Singapore National Research Foundation under its Campus for Research Excellence And Technological Enterprise (CREATE) program. Authors thank the Facility for Analysis, Characterization, Testing, and Simulation (FACTS) in Nanyang Technological University. The computational work for this article was partially performed on resources of the National Supercomputing Center, Singapore (<http://www.nscg.sg>).

Author contributions

Z.J.X. and Y.S. proposed the research and designed the experiments. Y.S. conducted modeling and simulation. J.W., S.X., J.S., S.Luo, J.G., S.S., and Y.C. carried out the experiments. S.X. conducted XAS characterizations. Y.S. wrote the manuscript. J.H., S.Li, X.W., and Z.J.X. performed the analysis and revised the manuscript.

Competing interests

The authors declare no competing interests.

Additional information

Supplementary information The online version contains supplementary material available at <https://doi.org/10.1038/s41467-023-38017-3>.

Correspondence and requests for materials should be addressed to Zhichuan J. Xu.

Peer review information *Nature Communications* thanks Tanja Kallio and the other anonymous reviewer(s) for their contribution to the peer review of this work.

Reprints and permissions information is available at <http://www.nature.com/reprints>

Publisher's note Springer Nature remains neutral with regard to jurisdictional claims in published maps and institutional affiliations.

Open Access This article is licensed under a Creative Commons Attribution 4.0 International License, which permits use, sharing, adaptation, distribution and reproduction in any medium or format, as long as you give appropriate credit to the original author(s) and the source, provide a link to the Creative Commons license, and indicate if changes were made. The images or other third party material in this article are included in the article's Creative Commons license, unless indicated otherwise in a credit line to the material. If material is not included in the article's Creative Commons license and your intended use is not permitted by statutory regulation or exceeds the permitted use, you will need to obtain permission directly from the copyright holder. To view a copy of this license, visit <http://creativecommons.org/licenses/by/4.0/>.

© The Author(s) 2023